ACS SyntheticBiology

Research Article

pubs.acs.org/synthbio

Load Capacity Improvements in Nucleic Acid Based Systems Using Partially Open Feedback Control

Vishwesh Kulkarni,*[,†] Evgeny Kharisov,[‡] Naira Hovakimyan,[§] and Jongmin Kim[∥]

[†]Institute of Systems and Synthetic Biology, Evry 91030, France

[‡]Department of Aerospace Engineering, University of Illinois, Urbana−Champaign, Illinois 61801, United States

[§]Department of Mechanical Science and Engineering, University of Illinois, Urbana−Champaign, Illinois 61801, United States

[∥]Division of Biology and Biological Engineering, California Institute of Technology, Pasadena, California 91125, United States

Supporting Information

ABSTRACT: Synthetic biology is facilitating novel methods and components to build *in vivo* and *in vitro* circuits to better understand and re-engineer biological networks. Recently, Kim and Winfree have synthesized a remarkably elegant network of transcriptional oscillators *in vitro* using a modular architecture of synthetic gene analogues and a few enzymes that, in turn, could be used to drive a variety of downstream circuits and nanodevices. However, these oscillators are sensitive to initial conditions and downstream load processes. Furthermore, the oscillations are not sustained since the inherently closed design suffers from enzyme deactivation, NTP fuel exhaustion, and waste product build up. In this paper, we show that a partially open architecture in which an $\mathcal{L}_1$ adaptive controller, implemented inside an *in silico* computer that resides outside the wet-lab apparatus, can ensure sustained tunable oscillations in two specific designs of the Kim−Winfree oscillator networks. We consider two broad cases of operation: (1) the oscillator network operating in isolation and (2) the oscillator network driving a DNA tweezer subject to a variable load. In both scenarios, our simulation results show a significant improvement in the tunability and robustness of these oscillator networks. Our approach can be easily adopted to improve the loading capacity of a wide range of synthetic biological devices.

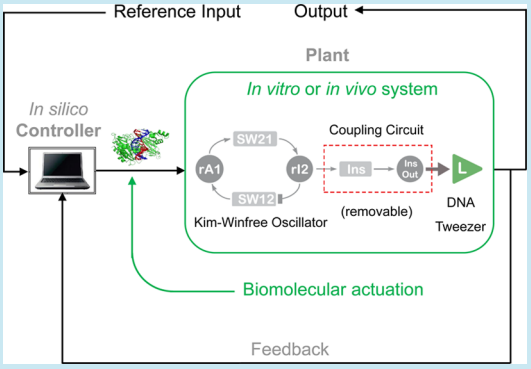

KEYWORDS: *molecular programming, nucleic acid circuits, DNA strand displacement, genelet, feedback, adaptive control, load capacity improvement*

Systems synthesized from DNA strands *in vitro* have made significant progress toward complex architecture with a predictable outcome.[3−6] By utilizing modular and predictable Watson−Crick base pairing rules as well as the strong catalytic activity of enzymes, switch motifs with sharp threshold responses and several circuit motifs have been demonstrated.[1,7−9] DNA-based circuits relying on predictable thermodynamics and kinetics of DNA strand interactions impart flexibility in synthesizing synthetic biological constructs and in coupling these circuits to *in vivo* processes (see refs 10−13 and references therein). For example, a biochemical oscillator can be successfully synthesized using a simplified experimental model of gene regulatory networks that utilizes DNA polymerase, nicking enzyme, and exonuclease to process the catalytic events.[13] In general, however, rendering these oscillators robust to loading effects arising from coupled downstream load processes is an important open problem.[1,14] In this paper, we propose a solution to this problem for the specific case of the synthetic Kim−Winfree oscillator network, illustrated in Figure 1A, which is a simple but effective coupled oscillator system in which two DNA switches SW_{12} and SW_{21} are coupled through activator and inhibitor blocks realized by RNA signals and auxiliary DNA species.[8]

We consider two cases: the Kim−Winfree oscillator network operating in isolation, and the Kim−Winfree oscillator network driving a DNA tweezer as a variable load process as described in ref 1. Even in isolation, the oscillator network is not very robust to the accumulation of interfering RNA waste products such that the oscillations slow down after each cycle and eventually ceases to operate due to enzyme inactivation, NTP fuel exhaustion, and buildup of wastes.[8] Further, the amplitudes and periods of oscillations exhibit limited tunability depending on the initial parameter choices. In ref 1, these oscillators are used to drive conformational changes of a DNA nanomechanical device called DNA tweezers. These tweezers, which consist of two double-helical domains connected by a hinge, have two single-stranded hands that can bind to targeted oligonucleotide sequences such as RNA signal species and auxiliary DNA

Special Issue: IWBDA 2013

Received: January 31, 2014
Published: May 1, 2014

 © 2014 American Chemical Society dx.doi.org/10.1021/sb5000675 | *ACS Synth. Biol.* 2014, 3, 617−626

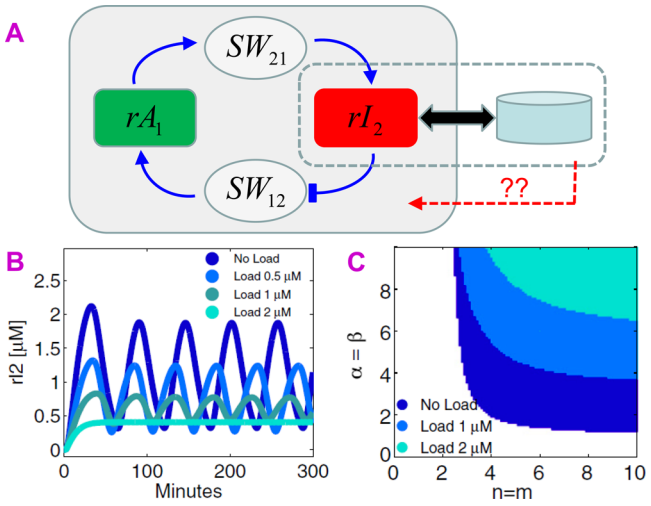

Figure 1. (A) Kim–Winfree oscillator network comprises two switches (SW_{12} and SW_{21}) connected through an activator rA_1 and an inhibitor rI_2 block. In ref 1, it is used to drive DNA tweezers. Because of the loading effects and a closed-system design, this network is unable to drive even moderate loads: the plot B (Reprinted with permission from ref 1. Copyright 2011 National Academy of Sciences) illustrates the loss of oscillations as the load increases from 0 nM to 2000 nM; as the plot C (Reprinted with permission from ref 1. Copyright 2011 National Academy of Sciences) illustrates, a mathematical analysis of a simplified model of the system shows that the allowable region in the parameter space for the existence of sustained oscillations diminishes as the load increases from 0 nM to 2000 nM. This highlights the need for more sophisticated controllers and for a more open design: for example, a design in which it is possible to inject a control input in a wet-lab setup. We propose the synthesis of such a system and present several simulation case studies.

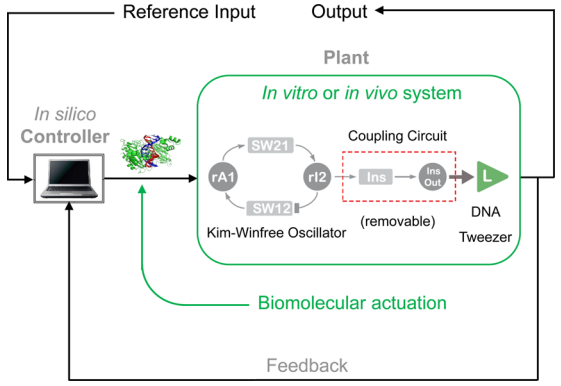

Figure 2. Our proposed partially open wet-lab system architecture. An $\mathcal{L}_1$ adaptive feedback controller is implemented inside an *in silico* computer that is physically separated from the wet-lab apparatus in which the synthetic biological system of interest is implemented. The controller takes the fluorescence read-out of the switch states as inputs. The controller output is the vector of the updated values of the inhibition constant K_I and the activation constant K_A. The system of interest to us, i.e., the plant, comprises a DNA tweezer load driven by a Kim–Winfree oscillator network. Here, the reference input is a vector whose components are the desired time-trajectories of the outputs of interest: in our case, the outputs of interest are the concentrations of (rA_1, rI_2) or ($T_{12}A_2$, $T_{21}A_1$). The fluctuating levels of rA_1 and rI_2 are used to open and close the DNA tweezer either directly or through a coupling unit. In contrast with the *in silico* controller architecture of ref 2 that uses a photonic actuation, we use a biomolecular actuation: specifically, the $\mathcal{L}_1$ controller output controls the concentration of DNA/RNA strands to be injected externally in the wet-lab apparatus.

species of the oscillator, thereby closing the tweezers. As Figure 1B,C shows, the oscillations degrade quickly with the amount of load and the oscillator cannot drive a load exceeding oscillator component concentrations. In ref 1, the challenge of reducing retroactivity from loading was addressed by inserting another DNA switch to amplify the signal to be propagated to the load process. However, this solution is not adequate for the case of uncertain and time-varying loads. In this paper, we propose an architecture and a feedback controller to overcome these limitations.

Our Main Contribution. A typical experimental realization of many synthetic biological devices today, including the Kim–Winfree oscillator network, is closed in the sense that once the operation starts, we do not either add any chemicals, especially NTP fuel, externally into the wet-lab apparatus or remove any chemicals, especially waste products, from the apparatus. Within the closed system, the oscillations are bound to die out sooner or later; diminishing NTP fuel eventually stops supporting the production of RNA signals and accumulating waste products clog down the toeholds and, as a result, adversely affect the signal propagation. Furthermore, the oxidation effects and the pH variations tend to deactivate the enzymes. Loading poses an additional challenge since it alters the system dynamics, increases the system order and the associated uncertainty. So, how should we improve the load capacity of such transcriptional devices? We answer this question by adopting a partially open architecture in the sense that it is possible to inject biomolecular species externally in the wet-lab apparatus but it is not possible to remove biomolecular material from the appartus. In addition, we propose a sophisticated *in silico* feedback controller, a block diagram of which is illustrated in Figure 2, which is to be coupled to the wet-lab apparatus. A light switching *in silico* controller, implementing a combination of a Kalman filter and a model predictive controller, was recently reported in ref 2. Our controller is an $\mathcal{L}_1$ adaptive controller that uses a DNA/RNA based actuation of the wet-lab apparatus.

The primary benefit of using a control theoretic approach is due to the fact that the wet-lab system comes with a fairly sizable uncertainty (owing to modeling simplifications and neglected chemical reactions) and time-varying signals such as disturbance, noise, and load (see refs 8 and 1 for details). As a result, a rigorous use of feedback is necessary to ensure that the performance objective is realized. Now, a number of feedback controllers can be synthesized, H^∞ controller, model predictive controller, model reference adaptive controller, PI controller, and so on. Indeed, a model predictive controller (combined with a Kalman filter) has recently been used in ref 2 to regulate *in vivo* gene expressions in *Saccharomyces cerevisiae* using a light-based actuation. In contrast, we propose an $\mathcal{L}_1$ adaptive controller and use a DNA/RNA strand based actuation that facilitates a much greater control channel bandwidth than the one provided by a light-based actuation. Broadly speaking, most of the currently used adaptive controllers aim to counter uncertainty at all possible frequencies whereas an $\mathcal{L}_1$ adaptive controller aims at a much more realistic goal of countering the uncertainty over a band of frequencies only.[15] For the Kim–Winfree oscillators, the uncertainty primarily needs to be countered in only a small band of frequencies: specifically, up to a few millihertz only since the period of oscillations is

dx.doi.org/10.1021/sb5000675 | *ACS Synth. Biol.* 2014, 3, 617–626

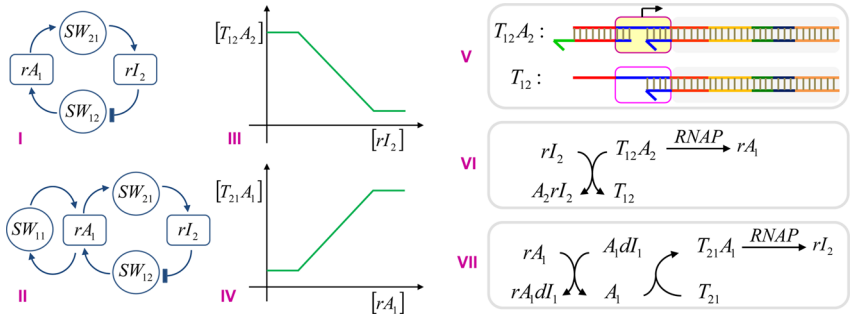

Figure 3. (I) Design I oscillator network of ref 8 comprises two switches, SW_{12} and SW_{21}, and two RNA regulatory signals, rA_1 and rI_2. A pointed arrow indicates production or activation and a blunt arrow indicates inhibition. As part V illustrates, the OFF state of the switch SW_{12}, denoted T_{12}, is a double-stranded DNA template with an incomplete single-stranded promoter for T7 RNAP and the ON state, denoted $T_{12}A_2$, is the complex obtained when A_2 completes T_{12}; likewise for the switch SW_{21}. (II) Design II of ref 8 has an additional switch SW_{11} that produces and is activated by rA_1. (III) Theoretical end-states of hybridization reactions in the absence of enzymes. As the input RNA inhibitor rI_2 concentration increases, initially the free DNA activator A_2 is consumed without affecting the switch state. When all free A_2 is consumed (i.e., $[rI_2] = [A_2^{tot}] - [T_{12}^{tot}]$), rI_2 displaces A_2 from the $T_{12}A_2$ complex in stoichiometric amounts until all A_2 is consumed (i.e., $[rI_2] = [A_2^{tot}]$), resulting in a piecewise linear graph (see Figure 1 of ref 8). (IV) The response of the switch SW_{21} to the activator rA_1 is piecewise linear as well. (VI) Injection of rI_2 turns SW_{12} off, which produces rA_1. (VII) Injection of rA_1 leads to the release of A_1 which turns SW_{21} on, which produces rI_2. As a result of parts VI and VII operating together, oscillations are produced in the network.

approximately 90 min. It can be proved mathematically as well that our $\mathcal{L}_1$ adaptive controller ensures that the wet-lab system exhibits oscillations that are robust over a quantifiable range of parametric changes, loads, disturbances, and uncertainties. The combination of dead-zone and saturation nonlinearities used by us (see the Supporting Information text) in processing measured biochemical concentrations has a far lower computational overhead than the one incurred by a Kalman filter used in ref 2. Furthermore, it can be proved that in many cases an $\mathcal{L}_1$ adaptive controller can be approximated by a much simpler PI controller which would further reduce the computational cost and render the controller implementable *in vitro* rather than *in silico*. As a result, we have opted for an $\mathcal{L}_1$ adaptive controller.

RESULTS AND DISCUSSION

System Description. The Kim−Winfree oscillator, derived recently in ref 8 and illustrated in Figure 3, uses bacteriophage T7 RNA polymerase (RNAP) and *Escherichia coli* ribonuclease H (RNase H). Several realizations of such an oscillator network are described in ref 8. In these synthetic transcription networks, transcriptional switch motifs are modularly wired into arbitrarily complex networks by changing the regulatory and coding sequence domains of DNA templates. We focus on the simplified models for the first two designs, viz., Design I and Design II, of the oscillator networks presented in ref 8, and the key elements in these networks are noted down in Table 1 and the key biochemical reactions are noted down in Table 2.

Oscillator Network: Design I. The oscillator network is illustrated in Figure 3,I. Each synthetic switch, denoted SW_{12} and SW_{21}, is controlled by an input signal, physically, an ssRNA strand, and produces an output signal, physically, an ssRNA strand. The OFF state of SW_{12}, denoted as T_{12}, consists of a double-stranded DNA template with an incomplete partially single-stranded promoter for T7 RNAP and its ON state is the complex $T_{12}A_2$ obtained when a single-stranded DNA activator A_2 completes the missing promoter region; $T_{12}A_2$ can be transcribed well, approximately half as efficiently as a full duplex template, likewise for the switch SW_{21}. Note that, at the molecular level, the input domain and the output domain are physically separated by the promoter region such that the independent choice of input and output sequences is guaranteed. The switch can be turned OFF by the addition of an inhibitor strand (either a single-stranded RNA rI_2 for the case of an inhibited switch or single-stranded DNA dI_1 for the case of an activated switch) which initiates binding at the toehold domain of the activator strand and displaces the activator A_j from the ON-state switch $T_{ij}A_j$. Free-floating inhibitor strands can also bind to complementary free-floating activator strands to form inert activator−inhibitor complexes. These annihilation reactions are important to establish adjustable activation and inhibition thresholds for target switches; the actual state change of switch templates are delayed until all the free-floating threshold species are consumed. Finally, the DNA activator strand A_1 can be released from the $A_1{\cdot}dI_1$ complexes when RNA activator strand rA_1 displaces dI_1 from $A_1{\cdot}dI_1$ through toehold-mediated strand displacement reaction. The released activator A_1 is then available to activate the switch SW_{21}. The catalytic production and degradation reactions are mediated by two enzymes: RNAP and RNase H. RNAP produces RNA signals from ON-state switches that in turn regulate the state of target switches, while RNase H degrades RNA signals within RNA−DNA hybrid complexes undoing the regulatory action by RNA signals. Together, the RNA activator rA_1 activates the production of RNA inhibitor rI_2 by modulating switch SW_{21}, whereas RNA inhibitor rI_2, in turn, inhibits the production of RNA activator rA_1 by modulating switch SW_{12}, thereby forming a negative feedback loop. The inhibition and activation

Table 1. Notation for the Kim−Winfree Oscillator Circuit

symbol	meaning
$T_{12}A_2$	ON state of the switch SW_{12}
T_{12}	OFF state of the switch SW_{12}
$T_{21}A_1$	ON state of the switch SW_{21}
T_{21}	OFF state of the switch SW_{21}
A_1dI_1, rA_1dI_1, A_2rI_2	functionally inert activator−inhibitor complex
rI_2	free-floating ssRNA inhibitor
dI_1	free-floating ssDNA inhibitor
rA_1	free-floating ssRNA activator
A_1, A_2	free-floating ssDNA activator
$[x]$	concentration of a biomolecular species x
$[T_{ij}^{tot}]$	$[T_{ij}] + [T_{ij}A_j]$

dx.doi.org/10.1021/sb5000675 | ACS Synth. Biol. 2014, 3, 617−626

Table 2. Key Chemical Reactions in the Kim−Winfree Oscillator (See Reference 8)

activation	annihilation	RNAP
$T_{21} + A_1 \rightarrow T_{21}A_1$	$A_1 + dI_1 \rightarrow A_1dI_1$	$T_{21}A_1 \rightarrow T_{21}A_1 + rI_2$
$T_{12} + A_2 \rightarrow T_{12}A_2$	$rA_1 + dI_1 \rightarrow rA_1dI_1$	$T_{21} \rightarrow T_{21} + rI_2$
	$A_2 + rI_2 \rightarrow A_2rI_2$	$T_{12}A_2 \rightarrow T_{12}A_2 + rA_1$
		$T_{12} \rightarrow T_{12} + rA_1$
inhibition	**release**	**RNase H**
$T_{21}A_1 + dI_1 \rightarrow T_{21} + A_1dI_1$	$A_1dI_1 + rA_1 \rightarrow rA_1dI_1 + A_1$	$rA_1dI_1 \rightarrow dI_1$
$T_{12}A_2 + rI_2 \rightarrow T_{12} + A_2rI_2$		$A_2rI_2 \rightarrow A_2$

thresholds can be established by adjusting the concentrations of free-floating threshold species, which in effect, sets delays in signal propagation. A negative feedback loop with appropriate delays can result in sustained oscillations in the chemical concentrations of rA_1 and rI_2 as well as the state of switch SW_{21} and SW_{12}. The key hybridization reactions are summarized in Table 2. Design II, illustrated in Figure 3,II, is obtained from Design I by adding a switch SW_{11}, which takes rA_1 as its regulatory activating input and produces rA_1 as its output.

Design I and Design II: Ordinary Differential Equation (ODE) Models. We shall first note our ODE model for Design I; this model is derived in ref 8 and the modeling assumptions are summarized in the Supporting Information text. Let us refer to this model as Model I. As shown in ref 8, this system can be represented using the following ODEs:

$$\frac{d[rA_1]}{dt} = k_p[T_{12}A_2] - k_d[rA_1] \quad (1)$$

$$\frac{d[rI_2]}{dt} = k_p[T_{21}A_1] - k_d[rI_2] \quad (2)$$

$$\frac{d[T_{12}A_2]}{dt} = \frac{1}{\tau}\left([T_{12}^{tot}]\frac{1}{1+\left(\frac{[rI_2]}{K_I}\right)^n} - [T_{12}A_2]\right) \quad (3)$$

$$\frac{d[T_{21}A_1]}{dt} = \frac{1}{\tau}\left([T_{21}^{tot}]\left(1 - \frac{1}{1+\left(\frac{[rA_1]}{K_A}\right)^m}\right) - [T_{21}A_1]\right) \quad (4)$$

where $[I]$ denotes the molecular concentration of a given biomolecular entity I. Let x^T denote the transpose of a given vector x. Then this model can be expressed in the form $\dot{x} = f(x, u)$, where $\dot{x} = dx/dt$ denotes the derivative of x with respect to time, x is a vector of the state variables, i.e., the switch states and the activator/inhibitor concentrations, given by $x = [rA_1\ rI_2\ T_{12}A_2\ T_{21}A_1]^T$, the control input u is given by $u = [K_I\ K_A]^T$, and $f(\cdot,\cdot)$ is a nonlinear function described by eqs 1−4. In the above equations, k_p represents the first-order rate constant based on RNAP, which produces RNA outputs, while k_d represents the first-order rate constant based on RNase H, which results in the degradation of RNA signals, τ is a relaxation time for the hybridization reactions, K_A is the activation threshold for the RNA activator rA_1, K_I is the inhibition threshold for the RNA inhibitor rI_2, and $[T_{ij}^{tot}]$ is the sum of concentrations of all molecular species containing T_{ij}. Assuming fast and irreversible hybridization reactions among the nucleic acid species, reasonable approximations for the thresholds are $K_I \approx [A_2^{tot}] - {}^1/_2\ [T_{12}^{tot}]$ and $K_A \approx [dI_1^{tot}] - [A_1^{tot}] + {}^1/_2\ [T_{21}^{tot}]$, while reasonable approximations for Hill exponents are $n \approx 4\ (K_I/[T_{12}^{tot}])$ and $m \approx 4\ (K_A/[T_{21}^{tot}])$. Hill exponents between 3 and 6 for steady-state switch responses were measured experimentally in ref 7. The ODE model for Design II can be obtained similarly and is described in the Supporting Information text; we refer to that model as Model II.

ODE Model: Accounting for the Loading Effects. Suppose Design I of the Kim−Winfree oscillator is used to drive the DNA tweezer by coupling rI_2 to the load L (see the inset "*in vitro* or *in vivo* system" of Figure 2). Here, rI_2 binds to L to form an active complex L^a as per $rI_2 + L \rightarrow L^a$. The active complex L^a degrades back into L as per $L^a \rightarrow L$ if rI_2 is fully consumed and as per $L^a \rightarrow rI_2 + L$ if rI_2 is not consumed fully. Let us assume that $[L^{tot}] = [L] + [L^a]$ remains constant. We assume that the active load and the total load, i.e., $[L^a]$ and $[L^{tot}]$ are measured real-time, e.g., by fluorophore and quencher labels on DNA tweezer (see ref 1). The case of Design II driving a DNA tweezer load can be treated on the same lines. Both models have been described in detail in ref 1 and are summarized in the Supporting Information text. Briefly speaking, if Design I is coupled to the DNA tweezer, then its dynamics get altered as follows: eq 2 gets replaced by eq S.8 in the Supporting Information text; likewise, a similar adjustment is to be made for the case of Design II coupled to the DNA tweezer.

ODE Model: Accounting for Enzyme Deactivation, Waste Product Build-Up, Disturbances, and Modeling Uncertainties. With the enzyme deactivation, the strengths of activation and inhibition decrease, i.e., the values of k_p, k_d, and the Hill coefficients n and m decrease. With the waste products building up, the binding rates decrease since the waste products have a tendency to bind to the toeholds and hence, effectively, the signal propagation degrades and the value of the time constant τ increases. The disturbances arise primarily due to temperature changes, pH changes, and oxidation effects. The temperature changes affect the binding rates and hence alter the value of τ. The buffer exhaustion tends to make the system more acidic with time and hence leads to enzyme deactivation and thereby decreases the values of k_p, k_d, n, and m. The oxidation effects lead to enzyme deactivation and hence alter the values of k_p, k_d, n, and m. The modeling uncertainty arises due to poorly characterized reaction rates and neglected chemical reactions. We account for those effects by adding a norm-bounded additive term to the ODEs describing the time-evolution of all state variables. The limitations imposed by NTP fuel exhaustion do not necessarily apply since we adopt a partially open architecture in which it is possible to inject chemicals into the wet-lab system.

We assume that the switch states, $[rA_1]$ and $[rI_2]$ are measured real-time with minimal measurement errors. We further assume that the nominal values of the enzyme constants k_p and k_d, and the binding constants k_r and k_f are known and that their degradation with time occurs exponentially; the constants k_p and k_d have already been described whereas the

dx.doi.org/10.1021/sb5000675 | ACS Synth. Biol. 2014, 3, 617−626

constants k_r and k_f are described in the Supporting Information text in the context of a DNA tweezer load. A rationale for the exponential decay assumption comes from the fact that a time-independent death process is an approximation for the decay in the enzyme activity: as noted in ref 16, T7 RNAP exhibits poor catalytic stability in dilute systems which can be reasonably approximated as an exponential decay function. It should be noted though that our controller synthesis procedure is not sensitive to whether the decay is exponential or not. All modeling uncertainties (caused, in part, by neglecting some chemical reactions) are lumped together into the norm-bounded time-varying signals δ_i, and we set the bound on δ_i heuristically. Such a model of Design I driving a DNA tweezer is described in detail in the Supporting Information text.

Description of the *in Silico* Controller. Our *in silico* controller, mentioned in Figure 2 and described in detail in Figure 4, monitors $[T_{ij}A_j]$, $[rA_1]$, and $[rI_2]$ using fluorescence

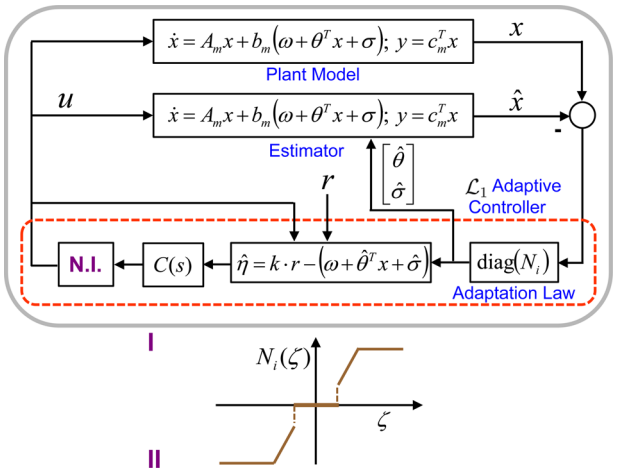

Figure 4. Our adaptive controller is implemented *in silico* in a computer outside the wet-lab apparatus and is then interfaced with the wet-lab apparatus. The controller takes the fluorescence read-out of the switch states as inputs. The controller output is the vector of the updated values of K_I and K_A. (I) Our $\mathcal{L}_1$ adaptive controller architecture. The block N.I. performs the nonlinearity inversion to generate the control inputs K_I and K_A; the nonlinearity inverted is the Hill-type activation/inhibition nonlinearity that exists due to the inhibition of $T_{12}A_2$ by rI_2 and the activation of $T_{21}A_1$ by rA_1. This, in effect, allows us to work with a linear plant model: e.g., the virtual control input $v_1 = 1/(1 + ([rI_2]/K_I)^n)$ inverts the inhibition nonlinearity and renders eq 3 as well as eq S.3 in the Supporting Information text linear in v_1. The linear plant model is either Model I or Model II, depending on which Kim−Winfree oscillator design is used, with the nonlinearity removed like so. Here, r is the vector of the reference inputs that $T_{12}A_2$ and $T_{21}A_1$ are to track. We chose the filter $C(s)$ by trial and error. (II) Each of the diagonal N_i nonlinearities is a combination of dead-zone and saturation nonlinearities; the non-linearities N_i are used to ensure stability and to reduce the controller chattering.

read-outs and controls the parameters K_I and K_A by injecting the threshold species A_1 and A_2 and their complements into the wet-lab system. It is straightforward to monitor the switch states by using fluorophore labels on switch templates T_{12} and T_{21} and quenchers on the activators A_1 and A_2: this allows real-time tracking of switch states as fluorescence read-out.[8] Hence, it is possible to design a feedback control system that can generate user-defined dynamics by monitoring switch states in real-time, calculating the deviations from the desired trajectories, and sending control inputs, A_j for positive inputs and its complement $\bar{A}_j$ for negative inputs, such that the switch states converge toward reference signals. To overcome the limitations of closed systems and to allow real-time fine-tuning of control inputs, we will assume a partially open architecture wherein inputs can be added with minimal volume change for the biochemical system under investigation. The feasibility of this approach was underscored in ref 7 wherein experimental perturbation of a two-switch network using activators and their complements as control inputs moved the network from a bistable parameter regime to a monostable regime and back.

We now describe how the controller is synthesized to achieve the following objective.

Objective: Ensure that the Kim−Winfree oscillators coupled to a variable load DNA tweezer exhibit the frequency of 0.001 rad/s and the amplitude of 40 nM around the baseline of 50 nM in $T_{12}A_2$ and $T_{21}A_1$ with the phase difference of $\pi/4$ rad.

Note that, typically, the Kim−Winfree oscillators have a time period of approximately 2 h (see Figure 3A of ref 8). So, realizing the above objective will also ensure that the Kim−Winfree oscillators behave similar to the experimental results. Since we use an advanced control theoretic approach to achieve this objective, we now briefly explain the basic controls concepts in the context of the Kim−Winfree oscillator.

Control Systems: Concepts and Terminology. Effectively, a controller is a black box that consumes controller inputs to produce controller outputs that are given as an input to the plant, i.e., the system that needs to be controlled; in this case, the plant is the Kim−Winfree oscillator operating either in isolation or under the load of a DNA tweezer. Here, the controller inputs are as follows: (I) reference input, the vector r of the desired oscillation waveforms for $T_{12}A_2$ and $T_{21}A_1$ and (II) measured plant output, the vector x of the fluorescence read-outs of all state variables (e.g., $T_{12}A_2$, $T_{21}A_1$, rI_2, and rA_1 are the state variables for the case of an isolated Model I while $T_{12}A_2$, $T_{21}A_1$, rI_2, rA_1, and L^a are the state variables for the case of Model I driving a DNA tweezer).

The controller output u is the vector $[K_I\ K_A]$ comprising the inhibition and activation constants. The controller objective is that, in the face of modeling uncertainties due to neglected chemical reactions, time-varying parameters, and poorly modeled kinetics, the following is ensured: (1) $T_{12}A_2$ and $T_{21}A_1$ reliably track their respective reference signals, and (2) the exogenous disturbances (due to thermal noise, enzyme deactivation, and waste product build up) are satisfactorily rejected.

A given system is termed static if its instantaneous output depends on its instantaneous input only. For example, logic gates such as the AND gate, the OR gate, and the XOR gate are static systems. A given system is termed dynamic if its instantaneous output depends on the values of the input at other time instants as well. For example, a linear system that takes the input u and generates the output y as per the differential eq 5 is a dynamic system:

$$\frac{dy}{dt} = -10y + u \tag{5}$$

A linear dynamic system, say H, is often expressed using its Laplace transform $H(s)$ since the Laplace transform well characterizes the frequency domain properties of linear systems. For example, the linear dynamic system H given by eq 5 is a low-pass filter and its Laplace transform is given as $H(s) = Y(s)/U(s) = 1/(s + 10)$. This system is a low-pass filter since,

dx.doi.org/10.1021/sb5000675 | ACS Synth. Biol. 2014, 3, 617−626

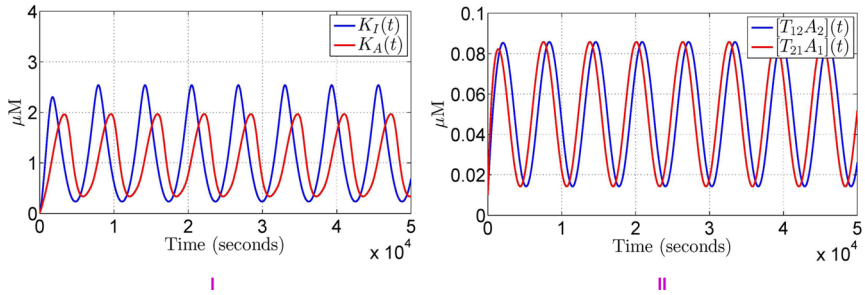

Figure 5. Simulation results for Scenario 1. Here, the parameter adaptation part of the $\mathcal{L}_1$-adaptive controller is turned OFF since there is no need for the adaptation. As the subplot I illustrates, the thresholds K_I and K_A are periodic. The subplot II illustrates that the desired oscillations are synthesized in the switch outputs $T_{12}A_2$ and $T_{21}A_1$.

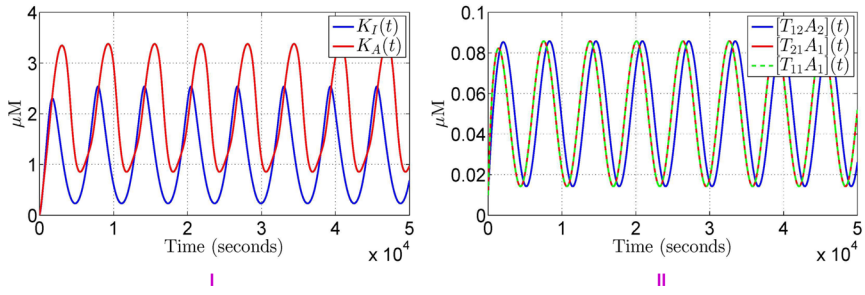

Figure 6. Simulation results for Scenario 2. Here, the parameter adaptation part of the $\mathcal{L}_1$-adaptive controller is turned OFF since there is no need for the adaptation. As the subplot I illustrates, the thresholds K_I and K_A are periodic. The subplot II illustrates that the desired oscillations are synthesized in the switch outputs $T_{12}A_2$ and $T_{21}A_1$.

roughly speaking, it attenuates all frequencies greater than 10 rad/s but does not attenuate any other frequency.

Synthesis of Our $\mathcal{L}_1$ Adaptive Controllers. In the Supporting Information text, an overview of an $\mathcal{L}_1$ adaptive controller synthesis for the generic case of controlling a plant featuring uncertain parameters is given, along with the details of how our $\mathcal{L}_1$ adaptive controller, illustrated in Figure 4,i, is synthesized. Here, we summarize the salient points. First consider Design I operating in isolation sans any modeling uncertainty, waste product build up, and enzyme deactivation, this model is described by eqs 1−4. Let r_1 denote the reference input for $T_{21}A_1$ and r_2 denote the reference input for $T_{12}A_2$. Then our reference input r is the vector $[r_1\ r_2]^T$ where $r_1(t) = 0.05 + 0.04 \sin(0.001t)$, $r_2(t) = 0.05 + 0.04 \sin(0.001t + \pi/4)$, where the units are in micromolar. The plant features a Hill-type saturation nonlinearities due to the inhibitory effect of rI_2 on $T_{12}A_2$ and the activating effect of rA_1 on $T_{21}A_1$. Since, by assumption, we can measure rA_1 and rI_2 and know K_I and K_A precisely, we can invert this nonlinearity using a virtual controller: e.g., the virtual control input $v_1 = 1/(1 + ([rI_2]/K_I)^n)$ inverts the inhibition nonlinearity and renders eq 3 as well as eq S.3 of the Supporting Information text linear in v_1. Then, the virtual control input $v_2 = 1-1/(1 + ([rA_1]/K_A)^m)$ inverts the activation nonlinearity and renders the equations describing the evolution of $T_{12}A_2$ and $T_{21}A_1$ linear (see the Supporting Information text). This allows us to use a linear dynamical system as our reference system and simplifies the synthesis procedure. The virtual control inputs are obtained by filtering the difference of the desired state r_i and the estimated parameter $\hat{\eta}_i$ using a suitable filter $C(s)$, which we choose on a trial and error basis; the bandwidth of $C(s)$ is chosen to be larger than 1.6 mHz, the reference signal frequency, so that a perfect robustness to the uncertainties and disturbances in the frequency range of interest, i.e., [0 mHz, 1.6 mHz], is achieved.

In the following simulation results, unless otherwise specified, the parameter adaption law is chosen as the nonlinearity N_i illustrated in Figure 4,ii and has the parameters $\Delta_\sigma = 10$, $dz_{\epsilon\sigma} = 0.000\,01$ while the lowpass filter $C(s)$ is chosen as $C(s) = ((1/(30s + 1))(1/(20s + 1))(1/(10s + 1)))$.

As chosen in ref 8, we set the nominal system parameter values as follows: $k_p = 0.04$/s, $k_d = 0.002$/s, $\tau = 500$ s, $n = m = 5$, $[T_{12}^{tot}] = [T_{21}^{tot}] = [A_1^{tot}] = 100$ nM, $K_A = K_I = 1$ μM. We set the initial condition of the plant to $x(0) = [0.1\ 0.1\ 0.1\ 0.1]^T$ and of the state predictor to $\hat{x}(0) = [0.1\ 0.1]^T$. In other words, the Kim−Winfree oscillator network is initialized to $rA_1(0) = 0.1$ μM, $rI_2(0) = 0.1$ μM, $T_{12}A_2(0) = 0.1$ μM, $T_{21}A_1(0) = 0.1$ μM.

Simulation Scenarios. The simulation results are obtained for two separate cases: (1) the feedback controller included with the parameter update law turned OFF (this facilitates only a partial benefit of our $\mathcal{L}_1$ adaptive controller) and (2) the feedback controller included with the parameter update law turned ON (this facilitates the full benefit of our $\mathcal{L}_1$ adaptive controller). We do not present the simulation plots for the case of the free running closed system, i.e., without an *in silico* feedback controller since, as expected, these do not exhibit robust and sustainable oscillations: all the same, these plots are presented for Scenario 4 (see Figure 9,i).

- Scenario 1: Nominal system of Design I, i.e., the system Design I with no uncertainty.
- Scenario 2: Nominal system of Design II, i.e., the system Design II with no uncertainty.
- Scenario 3: In real-world, the wet-lab system does exhibit uncertainty due to poor modeling, enzyme deactivations, waste product build up, etc. The model described in this scenario aims to account for it. It corresponds to the case wherein (1) the enzyme deactivations and the waste product build up have effectively slowed down the chemical reactions so that

dx.doi.org/10.1021/sb5000675 | ACS Synth. Biol. 2014, 3, 617−626

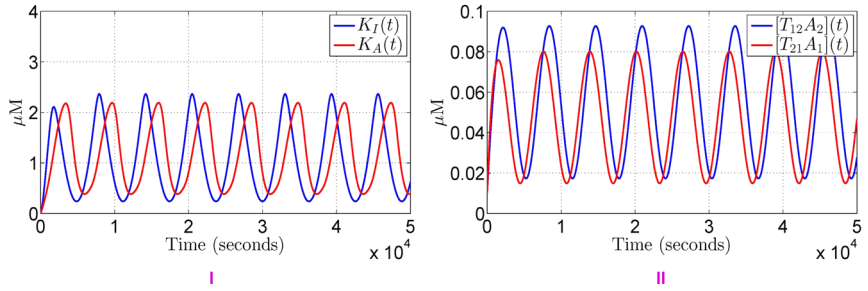

Figure 7. Simulation results for Scenario 3 with the parameter adaptation part of the $\mathcal{L}_1$-adaptive controller turned OFF. Now, the feedback controller is not very effective at compensating for the uncertainty as plots I and II illustrate. As the subplot II illustrates, the amplitudes of oscillations in $T_{12}A_2$ and $T_{21}A_1$ differ from each other.

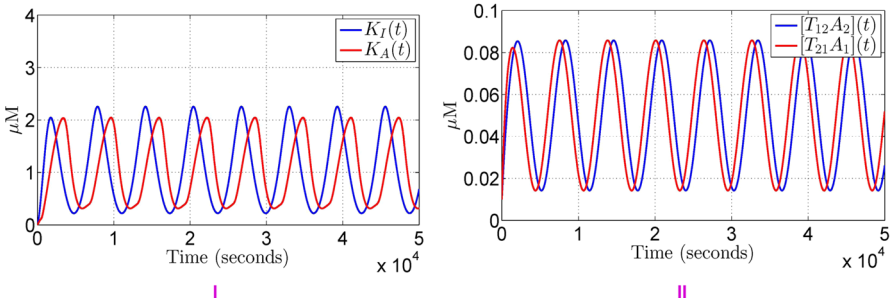

Figure 8. Simulation results for Scenario 3 with the parameter adaptation part of the $\mathcal{L}_1$-adaptive controller turned ON. Now, the feedback controller is effective at compensating for the uncertainty as plots I and II illustrate. As the subplot I illustrates, the thresholds K_I and K_A are periodic. The subplot II illustrates that the desired oscillations are synthesized in the switch outputs $T_{12}A_2$ and $T_{21}A_1$.

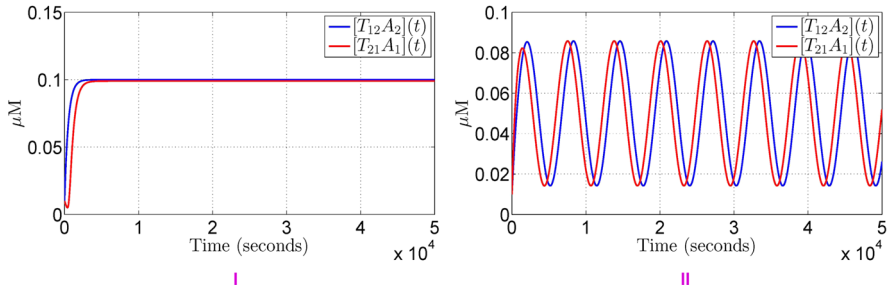

Figure 9. Simulation results for Scenario 4 and Scenario 5. (I) Scenario 4, if the $\mathcal{L}_1$ adaptive controller is not used then the free running system fails to generate any oscillations at all; this has been observed experimentally as well for high load cases (see ref 1). (II) However, if the $\mathcal{L}_1$ adaptive controller is used, then the desired oscillations are obtained even for the time-varying load considered in Scenario 5.

the time constant τ has increased from its nominal value 500 to 600 s, and furthermore, (2) we have underestimated $[T_{12}^{tot}]$ and overestimated $[T_{21}^{tot}]$ on an *a priori* basis. This is quantified as τ = 600 *s*, $[T_{12}^{tot}]$ = 0.11 μM, $[T_{21}^{tot}]$ = 0.095 μM.

- Scenario 4: Nominal system of Design I driving a constant DNA tweezer load of L = 1000 nM. Here, α = 0.76 μM, L^{tot} = 1 μM, k_r = 0.006/s, and k_f = 7900/M/s.
- Scenario 5: Nominal system of Design I driving a time-varying DNA tweezer load of $L = 1000 + 10\sin(0.001t)$ nM.
- Scenario 6: Nominal system of Design I speeded up by a factor of 5 to have the frequency of oscillations as 1 mHz.
- Scenario 7: Nominal system of Design I speeded up by a factor of 100 to have the frequency of oscillations as 20 mHz.

Simulation Results for Design I and Design II in Isolation. Since Scenario 1 and Scenario 2 concern the ideal case in which the system exhibits no uncertainty, there is no need to use parameter adaptation in the feedback controller. Indeed, as illustrated in Figures 5 and 6, our $\mathcal{L}_1$ controller is able to produce sustained oscillations in this scenario with its parameter update law turned OFF. If the adaptation law is turned OFF, then the $\mathcal{L}_1$ adaptive controller is not very effective against the parametric uncertainty as the simulation plots in Figure 7 illustrate. However, if the adaptation law is turned ON, then the $\mathcal{L}_1$ adaptive controller compensates for the uncertainty quite well as the simulation plots in Figure 8 illustrate.

Simulation Results for Design I Driving DNA Tweezer. We next consider the case of Design I driving a DNA tweezer for different values of the load L (viz., a constant load of L = 1000 nM and a time-varying load) in the presence of enzyme deactivation, NTP fuel exhaustion, and waste product build-up. The plant model is described in the Supporting Information text; here, the binding constants are k_r = 0.006/s and k_f = 7900/M/s. As the simulation results in Figure 9 illustrate, the Kim–Winfree oscillator under our $\mathcal{L}_1$ adaptive controller is able to

dx.doi.org/10.1021/sb5000675 | *ACS Synth. Biol.* 2014, 3, 617–626

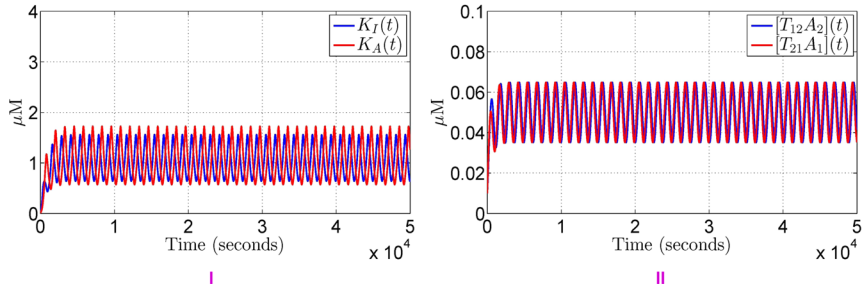

Figure 10. Simulation results for Scenario 6. Here, the reference signals are chosen to be $r_1(t) = 0.05 + 0.04 \sin(0.005t)$ μM, $r_2(t) = 0.05 + 0.04 \sin(0.005t + \pi/4)$ μM. If the parameter adaptation part of the $\mathcal{L}_1$-adaptive controller is turned ON, the feedback controller is effective at speeding up the oscillator by a factor of 5 as plot II illustrates, albeit the amplitude of oscillations has decreased by a factor of 2.

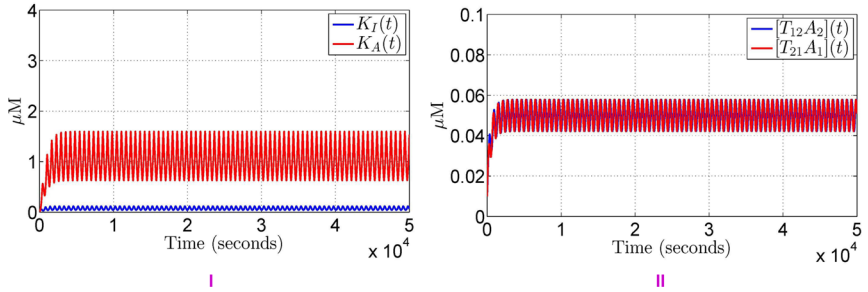

Figure 11. Simulation results for Scenario 7. Here, the reference signals are chosen to be $r_1(t) = 0.05 + 0.04 \sin(0.1t)$ μM, $r_2(t) = 0.05 + 0.04 \sin(0.1t + \pi/4)$ μM. If the parameter adaptation part of the $\mathcal{L}_1$-adaptive controller is turned ON, the feedback controller is not effective at speeding up the oscillator by a factor of 100 as plot II illustrates: even though $T_{12}A_2$ and $T_{21}A_1$ have the desired frequency of oscillations, the amplitude of oscillations is much smaller than the desired amplitude.

produce the desired oscillations on a sustained basis if the parameter update law is turned ON.

Speeding Up the Kim−Winfree Oscillator. For a variety of reasons, synthetic biological oscillators having a high frequency of oscillations are desirable. The frequency of oscillations in the Kim−Winfree oscillators, like many synthetic biological oscillators of today, is fairly low at 0.2 mHz. Our simulation results presented thus far show that our $\mathcal{L}_1$ adaptive controller can speed it up by a factor of 5 to 1 mHz (see Figure 10). This prompts the question: can we speed it up even further? It turns out that our controller is able to speed it up by a factor of 20 but runs into problems when the speed-up factor exceeds 100. However, if a greater speed-up is required then the nonlinearity to be inverted clips the saturation limits of the $\mathcal{L}_1$ adaptive controller and, as a result, the speed-up is achieved at the cost of the amplitude of the oscillations, which gets reduced by a factor of 4 (see Figure 11).

Potential Applications. *In vitro* synthetic biology approaches allow researchers to directly access and manipulate biomolecular parts without the overwhelming complexity and intertwined dependencies within *in vivo* cellular circuits.[17] Cell-free transcription and translation machineries can be encapsulated in lipid vesicles as a prototype for an artificial cell[18] and could be used to drive complex logic functions and cascades.[19] Recently, a 40-kbp long T7 phage genome with 60 genes was shown to be efficiently replicated in a cell extract,[20] resulting in a functional T7 phage produced in a completely cell-free environment. Furthermore, beyond simple illustrations of operating principles for nanomachines, the ability to control molecules at nanoscales could have applications in diverse technological areas. A straightforward and immediately realizable goal is interfacing with DNA-based structural motifs.[21,22] To illustrate the possibility of DNA structural motifs for drug-delivery nanovehicles for therapeutics, a DNA-based box was assembled with a lid that could be opened by strand displacement with a specific oligonucleotide key.[23] Therefore, these DNA-based nanostructures can be programmed to be responsive to external inputs to deliver their toxic cargoes in a specific fashion, while increasing the effectiveness of therapeutic action by surface display of the appropriate ligands.[24] A successful development for controlled molecular clocks can open the possibility of rendering these DNA-based nanostructures time-responsive.

CONCLUSION

Synthetic biology is growing as an expansion of the traditional biology discipline from natural organisms toward potential organisms.[25] Hence, making biological systems engineerable is a goal of engineers in the field of synthetic biology. Many technical and fundamental obstacles remain before the construction of synthetic biological systems can become routine. Because of the modular nature and programmable connectivity, DNA-based circuits operating in a simple *in vitro* environment offers a promising testbed for engineering biochemical systems. In ref 8, Kim and Winfree explored the DNA-based network for a wide range of parameters that resulted in an oscillatory response. However, these oscillations damp out eventually due to the limitations of closed systems. In particular, one of the experimental difficulty was the accumulation of short degradation products, which induced slow-down of oscillation periods and damping of oscillations. Detailed mechanistic modeling was also performed in ref 8 to gain a better understanding of the underlying biochemical system so that an appropriate controller to ensure the oscillations could be developed in a systematic manner. However, the progress on it has stalled since these detailed

dx.doi.org/10.1021/sb5000675 | *ACS Synth. Biol.* 2014, 3, 617−626

models are difficult to analyze owing to a surplus of nonlinearity and uncertainty. In a subsequent work,[1] the two-switch oscillator was connected to various downstream load processes, showing different extents of the system sensitivity depending on the amount of load processes and the mode of coupling. In this work, a partially open architecture was used to overcome the limitation of the closed systems and to allow real-time insertion of reference signals. This would allow a more predictable system behavior with robust and sustained oscillations, making the proposed simple ODE model as a reasonable description of the oscillator network. In this paper, we have shown that a partially open architecture in which an $\mathcal{L}_1$ adaptive controller, implemented in an *in silico* controller, is coupled to the wet-lab apparatus through a biomolecular actuation imparts tunability and robustness to the simplified models of Design I and Design II of the Kim−Winfree oscillator networks. The feedback controller is used to ensure that (1) the system tracks the reference command satisfactorily and (2) rejects the modeling uncertainties and exogenous disturbances satisfactorily. It may be noted that an open architecture such as a microchemostat platform[26] can relieve an important constraint imposed by waste build-up; however, the open architecture by itself cannot impart robustness to exogenous disturbances such as loading of circuits. As our simulation results illustrate, this approach ensures robustness to modeling uncertainties (e.g., due to unmodeled or neglected biomolecular reactions), time-varying parameters, and time-constants (e.g., because of enzyme deactivation, NTP fuel exhaustion, and waste product build up), and exogenous disturbances (e.g., thermal noise, uncertainty in DNA strand binding, etc.) and, furthermore, improves the loading capacity. We have illustrated this for two applications: (1) the Kim−Winfree oscillator network operating in isolation and (2) the Kim−Winfree oscillator network driving a DNA tweezer as a variable load. We have presented simulation results for the case of the *in silico* controller driving ODE models of these applications and will shortly present the results for the *in silico* controller driving the true wet-lab system. This approach can be easily adopted to improve the robustness, tunability, and loading capacity of a wide range of synthetic biological devices.

■ ASSOCIATED CONTENT

Supporting Information

Comprises ODE models and a detailed explanation of the controller synthesis procedure. This material is available free of charge via the Internet at http://pubs.acs.org.

■ AUTHOR INFORMATION

Corresponding Author

*E-mail: vvk215@gmail.com.

Notes

The authors declare no competing financial interest.

■ ACKNOWLEDGMENTS

This research is supported, in part, by the NSF CAREER Award 0845650, NSF CCF Grant 0946601, NSF CCF Grant 1117168, NSF Award 0832824 (the Molecular Programming Project), and AFOSR. We thank Prof. Richard Murray (California Institute of Technology) for discussions and support. A part of this research was supported by a "Visiting Professor" research grant of the University of Evry at the Institute of Systems and Synthetic Biology (Evry Genopole, France).

■ REFERENCES

(1) Franco, E., Friedrichs, E., Kim, J., Jungmann, R., Murray, R., Winfree, E., and Simmel, F. (2011) Timing molecular motion and production with a synthetic transcriptional clock. *Proc. Natl. Acad. Sci. U.S.A. 108*, E784−E793.

(2) Milias-Argeitis, A., Summers, S., Stewart-Ornstein, J., Zuleta, I., Pincus, D., El-Samad, H., Khammash, M., and Lygeros, J. (2011) *In silico* feedback for *in vivo* regulation of a gene expression circuit. *Nat. Biotechnol. 29*, 1114−1116.

(3) Seelig, G., Soloveichik, D., Zhang, D. Y., and Winfree, E. (2006) Enzyme-free nucleic acid logic circuits. *Science 314*, 1585−1588.

(4) Zhang, D. Y., Turberfield, A. J., Yurke, B., and Winfree, E. (2007) Engineering entropy-driven reactions and networks catalyzed by DNA. *Science 318*, 1121−1125.

(5) Soloveichik, D., Seelig, G., and Winfree, E. (2010) DNA as a universal substrate for chemical kinetics. *Proc. Natl. Acad. Sci. U.S.A. 107*, 5393−5398.

(6) Qian, L., Winfree, E., and Bruck, J. (2011) Neural network computation with DNA strand displacement cascades. *Nature 475*, 368−372.

(7) Kim, J., White, K., and Winfree, E. (2006) Construction of an *in vitro* bistable circuit from synthetic transcriptional switches. *Mol. Syst. Biol. 2*, 68.

(8) Kim, J., and Winfree, E. (2011) Synthetic *in vitro* transcriptional oscillators. *Mol. Syst. Biol. 7*, 465.

(9) Subsoontorn, P., Kim, J., and Winfree, E. (2012) Ensemble bayesian analysis of bistability in a synthetic transcriptional switch. *ACS Synth. Biol. 1*, 299−316.

(10) Zhang, D. Y., and Seelig, G. (2011) Dynamic DNA nanotechnology using strand-displacement reactions. *Nat. Chem. 3*, 103−113.

(11) Padirac, A., Fujii, T., and Rondelez, Y. (2012) Nucleic acids for the rational design of reaction circuits. *Curr. Opin. Biotechnol. 24*, 1−6.

(12) Chen, Y. Y., and Smolke, C. D. (2011) From DNA to targeted therapeutics: bringing synthetic biology to the clinic. *Sci. Transl. Med. 3*, 106ps42.

(13) Montagne, K., Plasson, R., Sakai, Y., Fujii, T., Rondelez, Y. (2011) Programming an *in vitro* DNA oscillator using a molecular networking strategy. *Mol. Syst. Biol. 7*, 466.

(14) Del Vecchio, D., Ninfa, A. J., and Sontag, E. D. (2008) Modular cell biology: retroactivity and insulation. *Mol. Syst. Biol. 4*, 161.

(15) Hovakimyan, N. and Cao, C. (2010) $\mathcal{L}_1$ *Adaptive Control Theory*, Society for Industrial and Applied Mathematics, Philadelphia, PA.

(16) Arnold, S., Siemann, M., Scharnweber, K., Werner, M., Baumann, S., and Reuss, M. (2001) Kinetic modeling and simulation of *in vitro* transcription by phage T7 RNA polymerase. *Biotechnol. Bioeng. 72*, 548−561.

(17) Hockenberry, A. J., and Jewett, M. C. (2012) Synthetic *in vitro* circuits. *Curr. Opin. Chem. Biol. 16*, 253−259.

(18) Noireaux, V., Maeda, Y., and Libchaber, A. (2011) Development of an artificial cell, from self-organization to computation and self-reproduction. *Proc. Natl. Acad. Sci. U.S.A. 108*, 3473−3480.

(19) Shin, J., and Noireaux, V. (2012) An *E. coli* cell-free expression toolbox: application to synthetic gene circuits and artificial cells. *ACS Synth. Biol. 1*, 29−41.

(20) Shin, J., Jardine, P., and Noireaux, V. (2012) Genome replication, synthesis, and assembly of the bacteriophage T7 in a single cell-free reaction. *ACS Synth. Biol. 1*, 408−413.

(21) Rothemund, P. W. K. (2006) Folding DNA to create nanoscale shapes and patterns. *Nature 440*, 297−302.

(22) Douglas, S. M., Dietz, H., Liedl, T., Högberg, B., Graf, F., and Shih, W. M. (2009) Self-assembly of DNA into nanoscale three-dimensional shapes. *Nature 459*, 414−418.

(23) Andersen, E. S., Dong, M., Nielsen, M. M., Jahn, K., Subramani, R., Mamdouh, W., Golas, M. M., Sander, B., Stark, H., Oliveira, C. L., Pedersen, J. S., Birkedal, V., Besenbacher, F., Gothelf, K. V., and Kjems, J. (2009) Self-assembly of a nanoscale DNA box with a controllable lid. *Nature 459*, 73−76.
(24) Douglas, S. M., Bachelet, I., and Church, G. M. (2012) A logic-gated nanorobot for targeted transport of molecular payloads. *Science 335*, 831−834.
(25) Elowitz, M., and Lim, W. A. (2010) Build life to understand it. *Nature 468*, 889−890.
(26) Balagadde, F. K., You, L., Hansen, C. L., Arnold, F. H., and Quake, S. R. (2005) Long-term monitoring of bacteria undergoing programmed population control in a microchemostat. *Science 309*, 137−140.